Supplement of Atmos. Chem. Phys., 20, 7553–7573, 2020
https://doi.org/10.5194/acp-20-7553-2020-supplement

Atmospheric Chemistry and Physics
Open Access
EGU

Supplement of

Identifying a regional aerosol baseline in the eastern North Atlantic using collocated measurements and a mathematical algorithm to mask high-submicron-number-concentration aerosol events

Francesca Gallo et al.

Correspondence to: Allison C. Aiken (aikenac@lanl.gov) and Francesca Gallo (fgallo@lanl.gov)

SI.1. Wind direction and speed

The percentage of time that the wind was sampled from a particular direction during the summer and winter are reported in Table SI.1, as a function of the cardinal and intercardinal directions. During the summer and winter at C1 and S1, the winds dominantly come from the southwest and south. Minimal time periods were sampled when the wind was coming from the north and northwest.

During the summer, C1 and S1 were dominated by winds from southwest at 27.6% and 32.8% of the time, respectively. At C1, winds from the east at 14.6% and southeast at 15.0% were the next most dominant directions. At S1, winds from the east were also the next highest at 21%, while the southeast wind direction was sampled less often at 8.2%. Winds from the north and northwest were the least frequent at C1 and S1: north at 7.3% (C1) and 6.9% (S1), northwest at 6.7% (C1) and 5.6% (S1).

In the winter, the wind had an almost equally dominant contributions from the south, at 29.0% (C1) and 30.3% (S1), and southwest, at 30.9% (C1) and 30.8% (S1). At C1 the next largest wind directions sampled were from the west at 17.6% and from the southeast at 12.6%. S1 differed from C1 in that, while the next most dominant wind direction was from the southeast at 19.4%, the wind from the west was significantly less at 7.4%. In contrast to the summer, both sites had a negligible contribution (≤ 12%) from the wind directions associated with the direction of the shore that equates to half of the wind rose: northwest, north, northeast, and east. While these wind directions were also not the dominant wind directions in the summer, the difference was that the winds were more equally distributed in the summer at 40.3% (C1) and 41.8% (S1) from the northwest to east.

Table SI.1. Percentage of time sampled as a function of wind direction during summer and winter at C1 and S1.

Wind Direction	Summer		Winter	
	C1	S1	C1	S1
N	7.3%	6.9%	2.4%	2.9%
NE	11.7%	8.0%	2.0%	1.7%
E	14.6%	21.3%	2.3%	5.6%
SE	15.0%	8.2%	12.6%	19.4%
S	6.9%	10.6%	29.0%	30.3%
SW	27.6%	32.8%	30.9%	30.8%
W	10.3%	6.5%	17.6%	7.4%
NW	6.7%	5.6%	3.2%	1.9%

The frequency of wind speed sampled at ENA are shown as a function of wind direction in Fig. SI.1. In general, the surface wind speed was higher at C1 than at S1, independent of the season. In the summer (Fig. SI.1a, b), surface wind speed mean values and one standard deviations were 4.7 ± 2.3 m s^{-1} (C1) and 3.2 ± 1.6 m s^{-1} (S1). The maximum wind speed during the summer came from the southwest for both sites: 15.2 m s^{-1} (C1) and 10.0 m s^{-1} (S1).

In the winter (Fig. SI.1c, d) the mean wind speeds at ENA was approximately double the speeds measured in the summer. The mean wind speed and standard deviations recorded were 7.3 ± 2.5 m s^{-1} (C1) and 5.7 ± 2.0 m s^{-1} (S1). The peak wind speed

measured during the winter was from the same direction as it was in the summer, from the southwest: 21.7 m s^{-1} (C1), 16.6 m s^{-1} (S1).

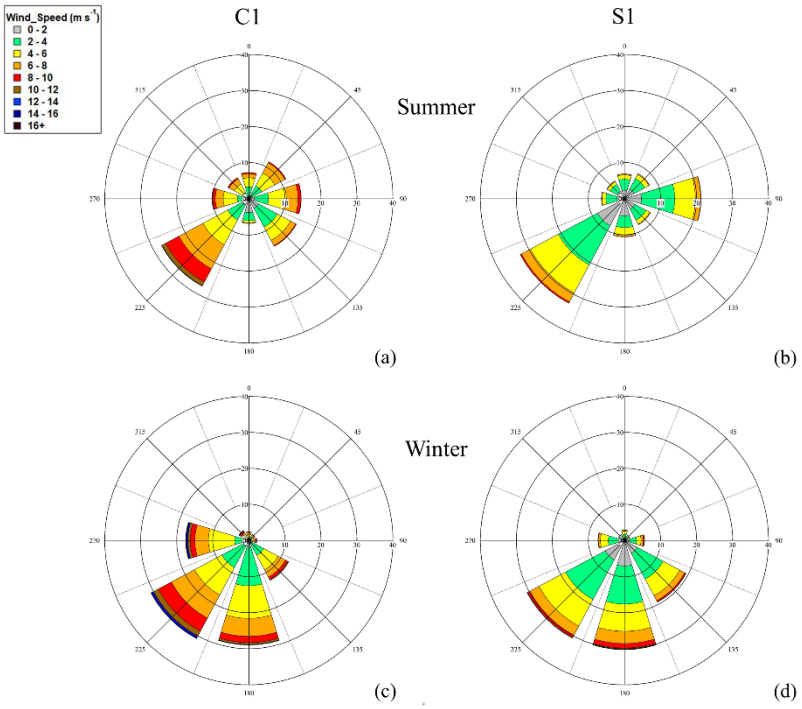

Figure SI.1. Surface wind rose plots during the summer (a, b) and winter (c, d) at C1 and S1. The length of the radial bars is the frequency of different wind speed ranges shown in colour, as a percentage of the time sampled.

The mean wind speeds observed at C1 and S1 were within 25% of each other during the summer and winter. The wind speed at C1 was higher during both seasons. S1 mean winds were 68% and 78% of C1 in the summer and winter, respectively. The observed maximum wind speed coincided with the dominant wind direction at C1 and S1 in both seasons. This observation was most evident in the summer when the wind was dominated by winds from the southwest. During the winter, there was a similar fraction of wind from the south and southwest with higher average wind speeds at both sites. Overall, C1 and S1 experienced similar dominant wind directions and mean wind speeds. We, therefore, expect C1 and S1 to exhibit similar trends in the aerosol data with the exception of the time periods when they are impacted by local aerosols that are not representative of the region. Those time periods should be influenced by the proximity, direction, size and type of the aerosol source in relation to the measurement site.

SI.2. Potential local aerosol sources at C1 and S1

While Graciosa Island and the location for C1 were selected due to the remote location and minimal population, the Graciosa regional airport is nearby. The airport regularly hosts two flights a day throughout the year, with one in the late morning or early afternoon and the other in the late afternoon. The largest nearby town is Santa Cruz, which is located ~1.8 km to the southeast of C1 with a population of ~1000. We identify potential local aerosol and trace gas sources associated with the airport and other local activities that may be relevant ENA spatially on a satellite image of the northeast section of Graciosa Island (Fig. SI.2).

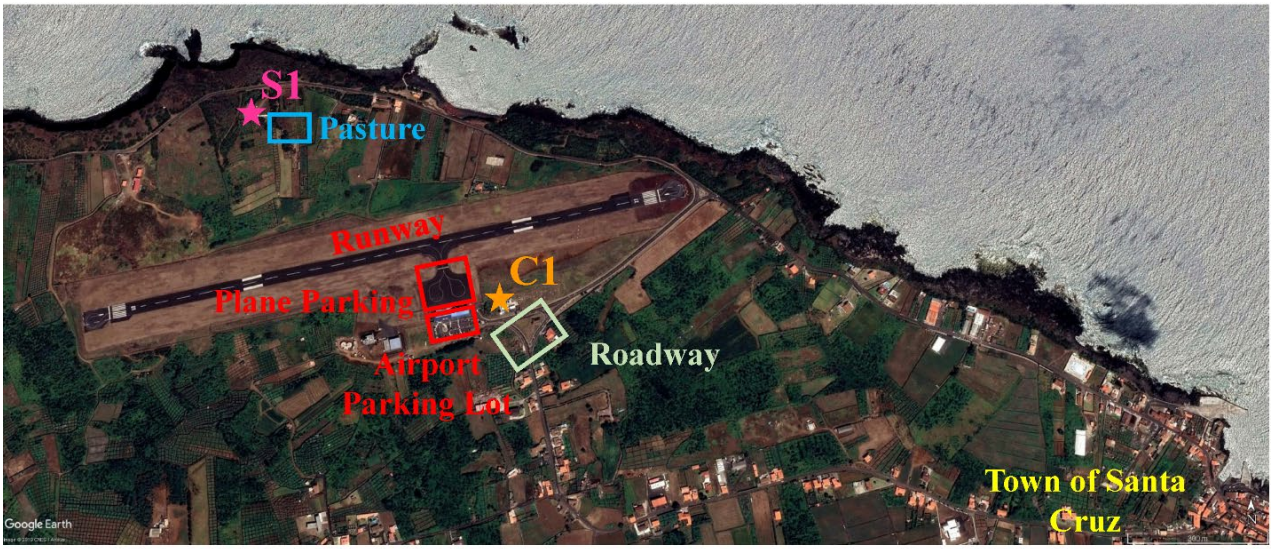

Figure SI.2. Satellite image with potential aerosol sources identified in the area surrounding ENA on Graciosa Island (© Google Earth).

The airport runway is located 116 m north of C1, spanning from the west to the northeast with regards to C1. The terminal building with one gate is located to the west. The airport parking lot is southwest of C1 and the aircraft parking area is to the west. The town of Santa Cruz is connected to the airport through a road to the east and south of C1.

S1 was located on the other side of the airport runway with respect to the location of C1. As such, the runway is located to the south of S1, spanning from the southwest to the southeast. A rural road that runs close to the shoreline is located to the north. An additional potential source at S1 includes a pasture where cows have been occasionally observed that is located to the east and southeast. A mobile diary unit with a diesel engine has also been observed on occasion in operation in association with the cows and the pasture. When present, the mobile dairy has been observed to operate two times a day for about an hour each time.

Identifying local aerosols at ENA based on proximity and wind direction of the source relative to the measurement site is complex since the sources originate over a wide variety of wind directions. We have attempted to summarize the known potential local aerosol sources in Table SI.2 as a function of their primary wind direction with regard to the locations of C1 and S1. Four nearby potential aerosol sources were identified at C1: the airport runway from the west to northeast, the road that connects Santa Cruz to the airport from east to south, the airport parking lot to the southwest, the airplane parking area to the west. At S1, the airport runway spans from the east to south and the rural road spans from the west to northeast. These were the two closest potential aerosol sources at S1. Additional potential sources identified near S1 included the pasture from the southeast to south and the decommissioned land fill with active vents to the southwest.

Table SI.2. Potential aerosol sources identified at ENA as a function of wind direction at C1 and S1.

Wind Direction	**Potential Aerosol Sources near ENA**	
	C1	**S1**
N	Airport runway	Rural road
NE	Airport runway	Rural road
E	Road	Airport runway, Rural road, Pasture

SE	Road	Airport runway, Pasture, Airplane and car parking, Road
S	Road	Airport runway
SW	Airport parking lot	Airport runway, Decommissioned landfill
W	Airport runway, Airplane parking	Rural road
NW	Airport runway	Rural road

Throughout this study, activities associated with the Graciosa airport that may impact aerosol measurements at ENA are collectively referred to as airport operations. Four known potential sources have been identified: aircraft assistance, runway maintenance, airport parking lot, road to the airport. While this is by no means an exhaustive list, further details on these known potential local aerosol sources at ENA are detailed here. Diesel engine vehicles assist aircraft operations before, during, and after landing and take-off. They assist with the loading and unloading of passengers and luggage during all stages before, during, and after the plane's time on the ground. Large vehicles with diesel engines are typically driven and parked several times daily in open spaces designated for plane loading and unloading to maintain the runway and in front of the airport terminal building. Once a day, between approximately 7:45 and 8:30 UTC, three trucks leave the warehouse west of the airport terminal building, and travel the length of the runway several times over a period of approximately 20 to 25 minutes before returning to the warehouse. The parking lot to the southwest of the airport is utilized mostly during times when planes are arriving and departing and to a lesser degree throughout the operational period of the airport. External to the airport, but still related, is the road that connects the town of Santa Cruz to the airport through an intersection located between the east and south side of the C1 site. While the area is rural, traffic is generally low, and there are no stoplights, increased traffic is observed before the arrival and after the departure of aircraft at the airport.

SI.3. Size distribution

Size distribution can be used to determine the source of high aerosol concentrations since different combustion sources, fuel types, and modes of operation produce different particle sizes. For example, depending on the jet fuel composition, aircrafts produce Aitken mode particles with D_p < 100 nm at number concentrations of ~ 4,000 – 30,000 cm^{-3} (Moore et al., 2017) that have been observed to be even greater during take-off and landing at ≥ 40,000 cm^{-3} (Campagna et al., 2016). Aerosol from port fuel injection gasoline vehicles have been measured to be ~ 10,000 cm^{-3} with mean D_p between 40 to 80 nm. The N_{tot} of particles emitted by diesel engines can be as high as 10^4 cm^{-3} with larger mean aerosol D_p between 60 and 120 nm, larger than those emitted by gasoline engines (Harris and Maricq, 2001). In general, combustion engines produce mean aerosol size distributions dominated by the Aitken mode. Smaller size distributions are attributed to more efficient combustion sources and shorter distances between the source and measurement site (Lighty et al., 2000).

In Fig. SI.3, we compare the measured size distributions from the UHSAS at C1 and S1 in the summer and winter. During the summer, the size distributions were similar in the number concentration and the mean mode D_p of 150 nm at both sites. A bimodal size distribution was evident, but the peak of the smaller mode was not able to be determined due to the UHSAS lower D_p limit. Despite not being able to size particles below D_p = 70 nm, the combined analysis presented in Section 4.1 enabled us to conclude that similar number concentrations of particles observed at C1 and S1 occurred above and below D_p = 70 nm. The main difference

observed between the measured size distributions at C1 and S1 in the summer was that there were 11% more particles from 80 nm to 150 nm at C1 than S1 (Fig. SI3.a).

In the winter, the bimodal structure was less evident at C1 and S1 (Fig. SI3.b). C1 had 38% more aerosol with D_p < 150 nm than S1. This difference was significantly larger than what was observed in the summer. The peak of the size distribution was also shifted to slightly smaller sizes than 150 nm at C1 than S1. This could have been due to the presence of more local sources with aerosols D_p < 150 at C1 than S1 in the winter and/or to different meteorological conditions than were observed in the summer. This difference in season was in agreement with Fig. 3 (Sect. 4.1) where a higher difference between N_{tot} was observed between C1 and S1 in the winter than in the summer.

During both summer and winter, C1 had more aerosol than S1 for D_p < 150 nm. This is likely due to the closer proximity of C1 to the Graciosa airport and the road to Santa Cruz. While the difference between the size distributions measured at C1 and S1 in the summer was minimal for D_p > 70 nm, we expect the difference would be more evident if sizing were available for D_p < 70 nm. We base this statement on the comparison of N_{tot} and N_{UHSAS} in section 4.1.

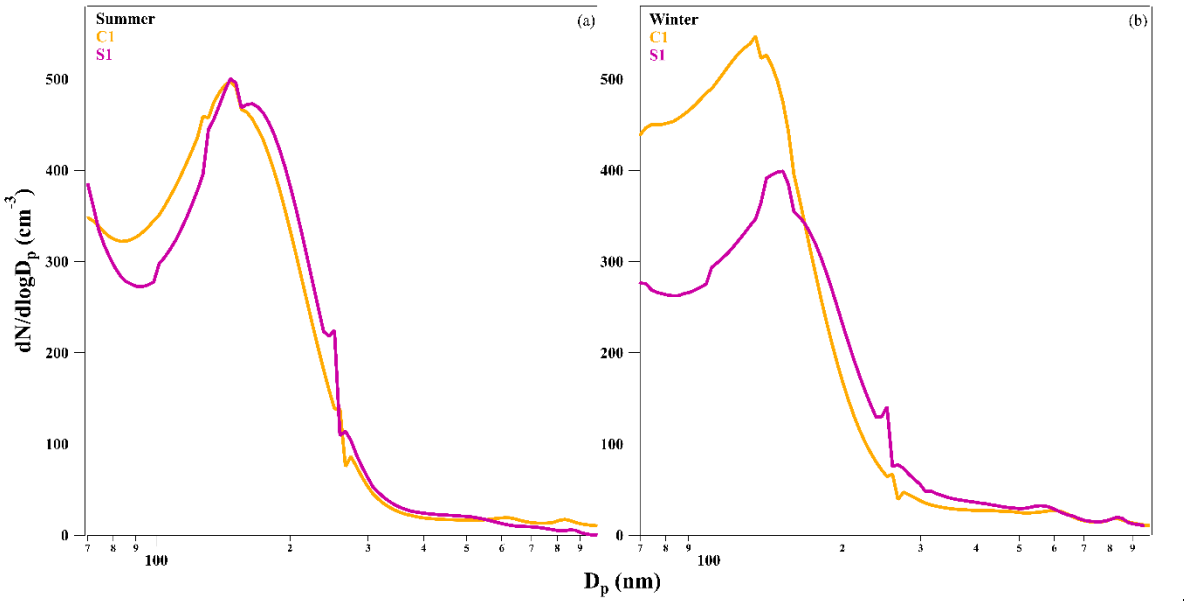

Figure SI.3. Aerosol size distributions at C1 (orange) and S1 (pink) during summer (a) and winter (b).

SI.4. Variability with wind direction

Mean N_{At} had the highest variability of all modes as discussed above. N_{At} and N_{Ac} had a larger observed variability in the winter than in the summer. For these reasons we evaluate the dominant submicron size modes as a function of wind direction to assess the variability in association with the direction of the known potential local aerosol sources identified in Section SI.2. N_{At} and N_{Ac} are plotted in Fig. SI.4 at C1 and S1 during the summer and winter.

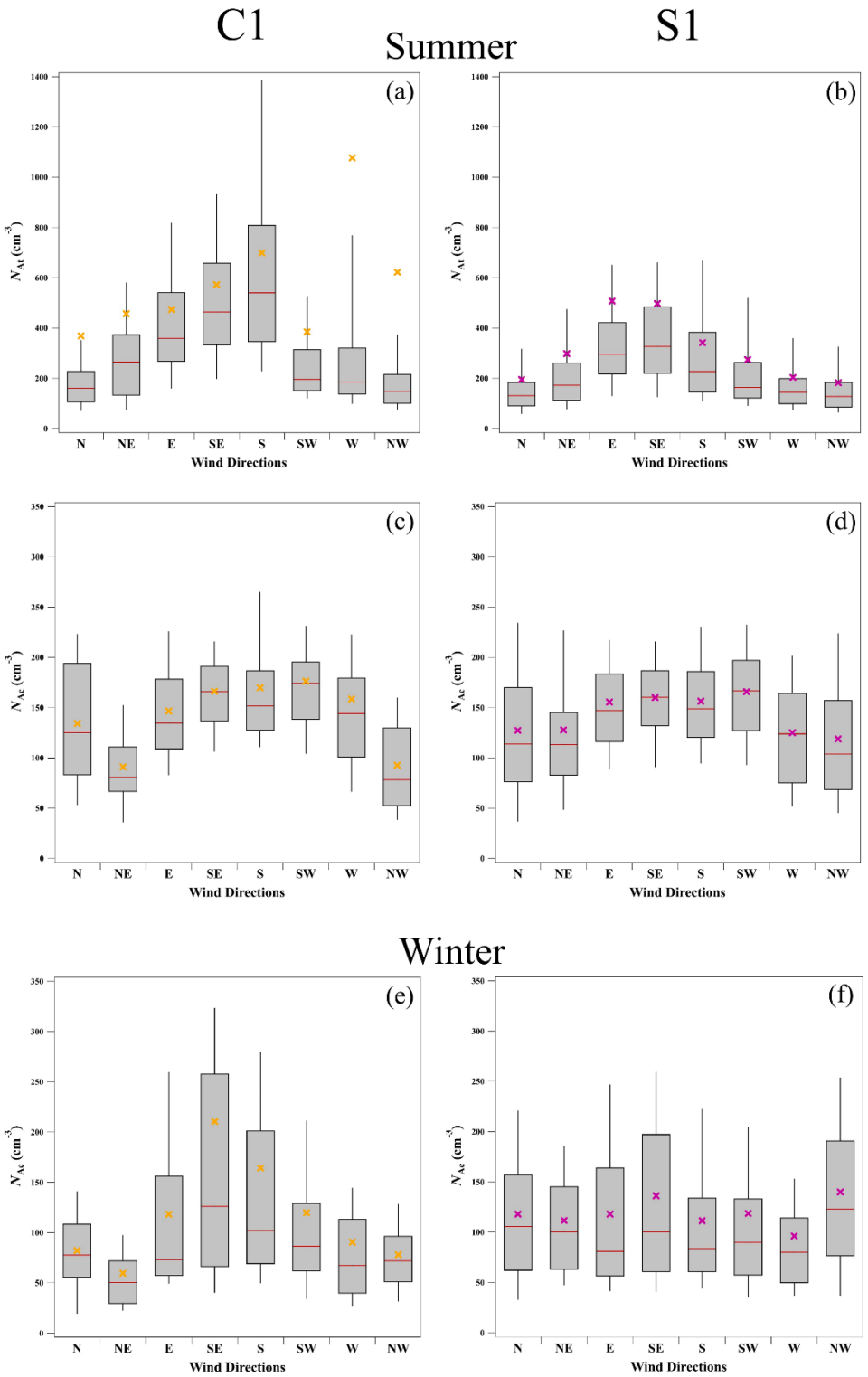

Figure SI.4. N_{At} (a,b) in the summer and N_{Ac} in the summer (c, d) and in the winter (e, f). Data is plotted as the function of wind direction (median red lines, mean x coloured by site) at C1 (orange) and S1 (pink). Box bottom: 25%, box top: 75%, whisker bottom: 10%, whisker top: 90%).

N_{At} at C1 (Fig. SI.4 a) had the highest deviation between the mean and median when the wind was coming from the west (mean: 1007 particles cm^{-3}, median: 185 particles cm^{-3}) and northwest (mean: 623 particles cm^{-3}, median: 148 particles cm^{-3}). N_{At} at C1 from the west and northwest are associated with the direction of the airport runway. Aircraft produce submicron aerosol of different

mean D_p during different modes of operation. Distinct aerosol size distributions centered at ~ 90 nm from nearby aircraft during landing and take–off, while a sub–30 nm mode has been observed to be prevalent during periods when aircraft are idling on the ground (Herndon et al., 2005). While we were not able to resolve these differences in the ENA dataset due to the lack of size information below 70 nm, we were able to confirm that the largest variability was observed in the smallest mode of particles shown here, N_{At}, when the wind was from the directions associated with the airport and its operation. N_{At} from the direction of the road to the airport, east to south, at C1 was not observed to have significantly higher variability that the other directions.

N_{At} at S1 had less variability between the mean and median when averaged over all wind directions in comparison to C1 in the summer (Fig. SI.4d). The highest variability in the data at S1 was associated with wind directions from the east (mean: 507 cm^{-3}, median: 294 cm^{-3}) and southeast (mean: 498 cm^{-3}, median: 326 cm^{-3}). The road and pasture were to the east and the airport runway, terminal and parking lot were to the southeast of S1.

Winter N_{At} at C1, not shown, exhibited a similar trend in regard to the summer data with the highest N_{At} coming from the west. N_{At} from the west had the highest mean of all the wind directions at 1650 cm^{-3} with a corresponding median an order of magnitude lower at 170 cm^{-3}. The deviation between the median and the mean was the greatest from the west during the winter, approximately a factor of two times greater than what was observed in the summer. The deviation in the mean and median when the wind was coming from the northwest was smaller than what was observed in the summer at C1. N_{At} was not available at S1 in the winter for comparison with C1, although we expect it would have had less variability.

As was observed in Fig. 4, N_{Ac} represented a smaller fraction of the total submicron aerosol at C1 and S1 with a lower variability between the median and mean N_{Ac}. Mean and median N_{Ac}, in Fig. SI.4 c, d, had a low variability across all wind directions at C1 and S1 in the summer. This is in contrast to what was observed for N_{At} during the same period. Mean N_{Ac} were between 92 and 170 cm^{-3} at C1, and the median N_{Ac} were between 78 and 174 cm^{-3}. Mean N_{Ac} were between 118 $cm^{-3}$and 165 cm^{-3} at S1 in the summer (Fig. SI.4 d). The median number concentrations are between 103 cm^{-3} and 166 cm^{-3}.

The largest variability of N_{Ac} at C1 was observed in the winter when the wind was from the southeast (mean: 210 cm^{-3}, median: 126 cm^{-3}) and south (mean: 164 cm^{-3}, median: 102 cm^{-3}) as is shown in Fig. SI.4 e. This variability was significantly below what was observed for N_{At} as a function of wind direction in the winter. Winter N_{Ac} at S1 (Fig. SI.4 f) had more variability between the median and mean N_{Ac} than what was observed in the summer. It was still significantly less than what was observed in the N_{At} in the summer. The largest variability in N_{Ac} at S1 in the winter was observed when the wind was from the east (mean: 123 cm^{-3}, median: 80 cm^{-3}) and southeast (mean: 140 cm^{-3}, median: 96 cm^{-3}). S1 data when compared to C1 had less variability across all wind directions and seasons, similar to what was observed when comparing N_{At} at C1 and S1.

In summary for the data shown here, N_{At} exhibited the highest variability represented as a high bias of the mean versus the median of all the submicron modes. The highest bias in the mean values in comparison to the medians was associated with the direction of airport operations at C1 (north and northwest) and S1 (east, southeast and south). At ENA the high N_{At} variability was most likely due to local combustion sources based on the size and the wind directions from which they were observed. This conclusion is supported by the fact that combustion sources are known to produce high concentrations of small mode particles with $D_p < 200$ nm. The high variability observed at ENA was mostly confined to the N_{At}, although was also observed in N_{Ac} during the winter. The main regional sources of N_{Ac} at ENA have been attributed to the entrainment of aerosol from the free troposphere and the

growth of N_{At} (Zheng et al. 2018). As such, the variability observed here within N_{Ac} in the winter likely includes these processes and local aerosol sources that were not observed in the summer. Chemical and optical property measurements collected by the AOS should be used in the future to further validate the aerosol sources associated with the variability observed here in the summer and winter.

SI.5. Comparison of ENA-AM to a smoothing algorithm

We applied a smoothing algorithm based on the one that Liu et al. (2018) developed for the AOS CPC during AWARE to our data at ENA. A 24-hour running median was used to mask the N_{tot} one-minute data collected during the summer at C1. Figure SI.5 shows a comparison between ENA C1 data filtered using ENA-AM and the smoothing method. After applying the smoothing algorithm 2% of the original data were retained.

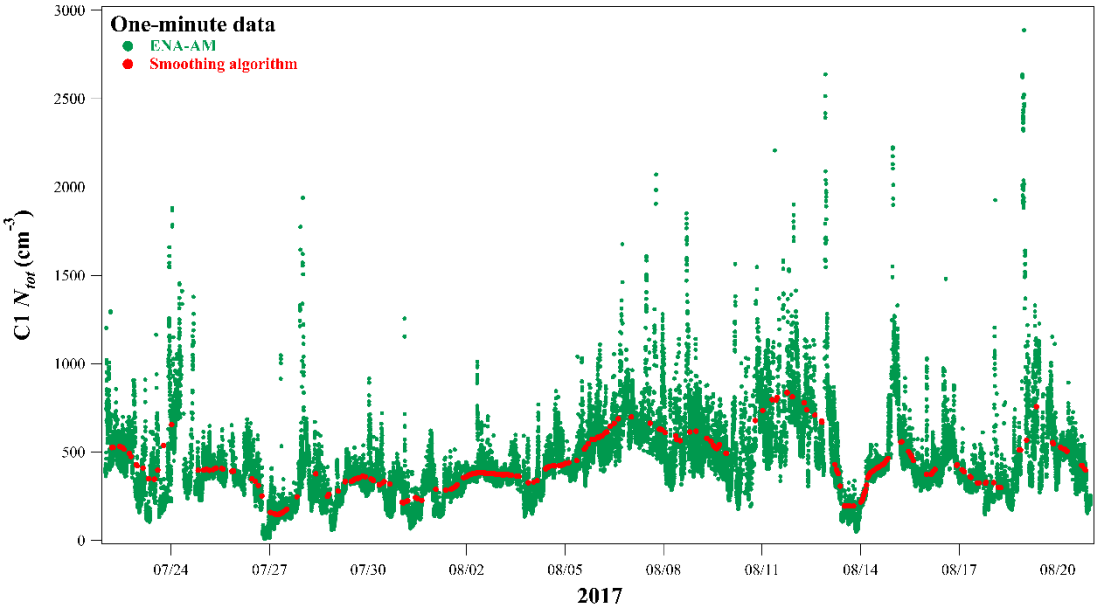

Figure SI.5. N_{tot} data at C1 in the summer after applying a 24-hour running median smoothing algorithm (red) and ENA-AM (green).

SI.6. Comparison of ENA-AM to the filter developed by Zheng et al. (2018)

We recreated the mask developed by Zheng et al. (2018) and we applied it to N_{tot} one-second data collected during our summer period. After applying the filter to the original one-second data, we averaged the data to a one-minute time base, masking the one-minute periods that included any masked data for comparison with ENA-AM. Figure SI.6 shows a time series of masked one-minute N_{tot} at C1. We observed that both masks were able to identify the high concentration aerosol events, however ENA-AM removed a lower amount of data.

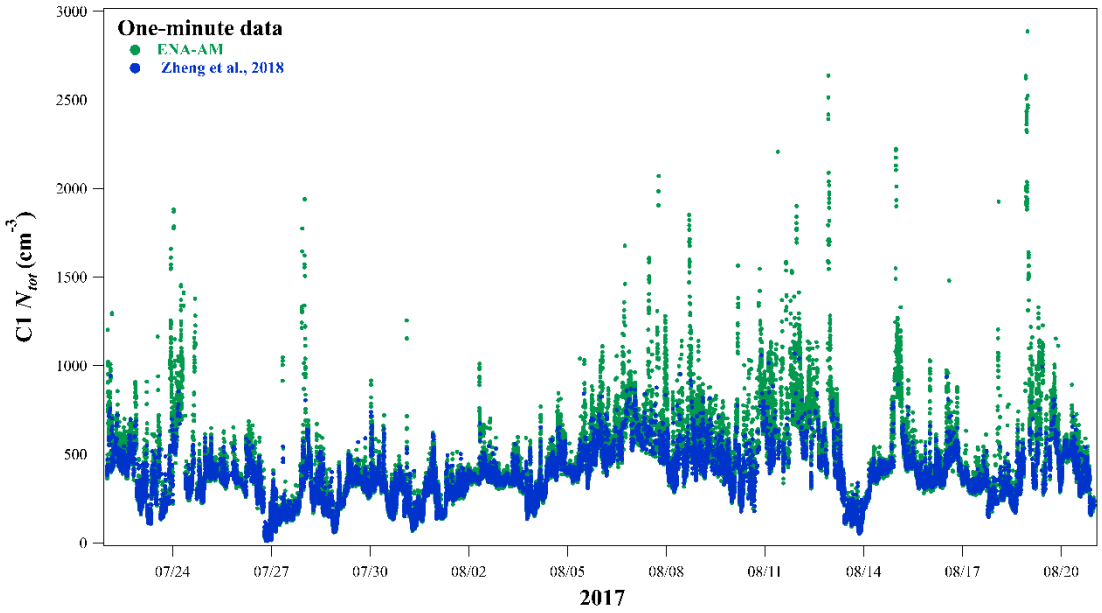

Figure SI.6. N_{tot} data at C1 in the summer after applying Zheng et al. (2018) method (blue) and ENA-AM (green).

The two masks agreed 68% of the time of the time and a high correlation between the masked datasets was generated (Fig. SI.7) with a slope of 0.976 and R^2 of 0.988. In this way, the Zheng et al. (2018) method masked a higher amount of data in the one-minute averaged dataset: 41% against the 26% masked by ENA-AM.

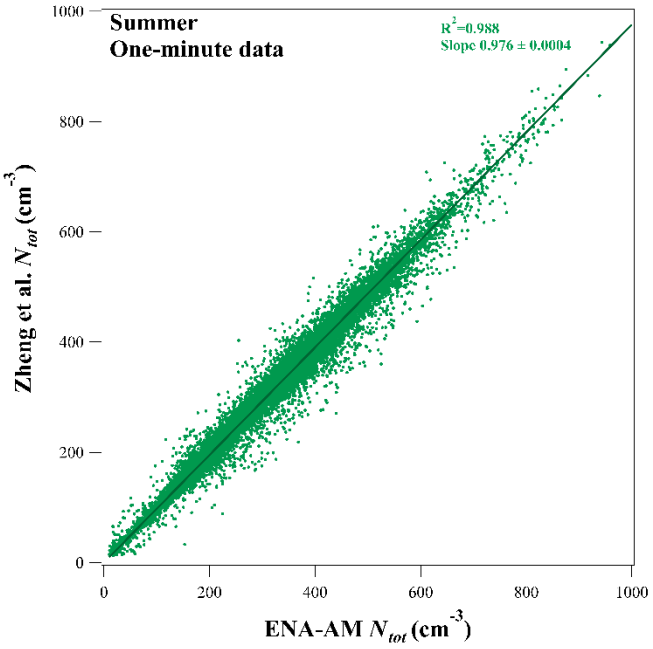

Figure SI.7. Scatter plot of Zheng et al. (2018) and ENA-AM masked one-minute N_{tot} data at C1 in the summer.

As hourly averages are often used to study seasonal trends and within models, we also investigated the application of both methods to N_{tot} data mapped onto a one-hour time base. Due to the amount of data points masked in N_{tot} one-minute, we averaged the remaining data points within each hour ignoring the masked data points. Without averaging the remaining data within each one-

hour time period, 74% of the data for ENA-AM and 96% of the data for Zheng's method would be removed. A slightly lower correlation (R^2 = 0.929 with a slope = 0.876 ± 0.005) was found between the masked one-hour N_{tot} datasets (Fig. SI.8). This larger deviation between the masks is a result of the lower percentage of data masked by ENA-AM which leads to higher hourly averages in comparison to the other method. The amount of data removed by the Zheng et al. (2018) method in N_{tot} one-hour masked datasets was 4% versus 0.5% removed by ENA-AM.

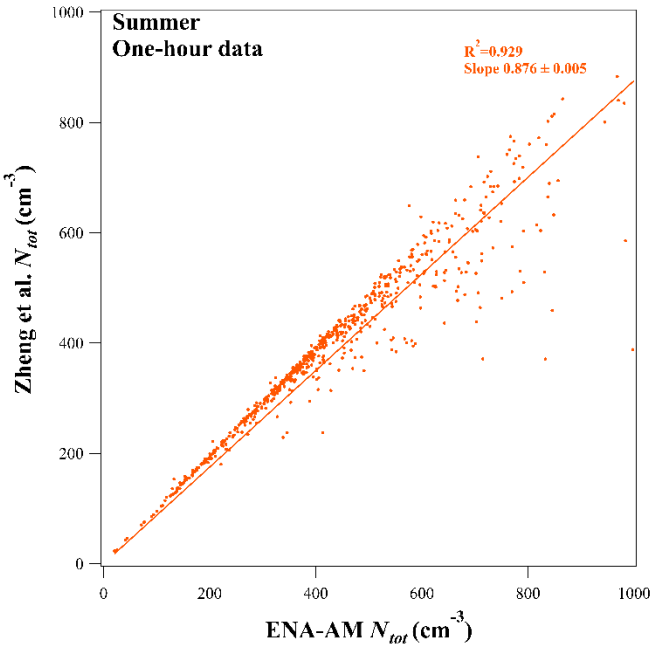

Figure SI.8. Scatter plot of Zheng et al. (2018) and ENA-AM masked one-hour N_{tot} data at C1 in the summer.

References:

Campagna, M., Frattolillo, A., Pili, S., Marcias, G., Angius, N., Mastino, C., Cocco, P., and Buonanno, G.: Environmental Exposure to Ultrafine Particles inside and nearby a Military Airport, Atmosphere, 7, 138, 10.3390/atmos7100138, 2016.

Harris, S. J., and Maricq, M. M.: Signature size distributions for diesel and gasoline engine exhaust particulate matter, Journal of Aerosol Science, 32, 749-764, https://doi.org/10.1016/S0021-8502(00)00111-7, 2001.

Herndon, S. C., Onasch, T. B., Frank, B. P., Marr, L. C., Jayne, J. T., Canagaratna, M. R., Grygas, J., Lanni, T., Anderson, B. E., Worsnop, D., and Miake-Lye, R. C.: Particulate Emissions from in-use Commercial Aircraft, Aerosol Science and Technology, 39, 799-809, 10.1080/02786820500247363, 2005.

Lighty, J. S., Veranth, J. M., and Sarofim, A. F.: Combustion Aerosols: Factors Governing Their Size and Composition and Implications to Human Health, Journal of the Air & Waste Management Association, 50, 1565-1618, 10.1080/10473289.2000.10464197, 2000.

Liu, J., Dedrick, J., Russell, L. M., Senum, G. I., Uin, J., Kuang, C., Springston, S. R., Leaitch, W. R., Aiken, A. C., and Lubin, D.: High summertime aerosol organic functional group concentrations from marine and seabird sources at Ross Island, Antarctica, during AWARE, Atmos. Chem. Phys., 18, 8571-8587, 10.5194/acp-18-8571-2018, 2018.

Moore, R. H., Shook, M. A., Ziemba, L. D., DiGangi, J. P., Winstead, E. L., Rauch, B., Jurkat, T., Thornhill, K. L., Crosbie, E. C., Robinson, C., Shingler, T. J., and Anderson, B. E.: Take-off engine particle emission indices for in-service aircraft at Los Angeles International Airport, Scientific data, 4, 170198-170198, 10.1038/sdata.2017.198, 2017.

Zheng, G., Wang, Y., Aiken, A. C., Gallo, F., Jensen, M., Kollias, P., Kuang, C., Luke, E., Springston, S., Uin, J., Wood, R., and Wang, J.: Marine boundary layer aerosol in Eastern North Atlantic: seasonal variations and key controlling processes, Atmos. Chem. Phys. Discuss., 2018, 1-36, 10.5194/acp-2018-574, 2018.